Cardiac Microlesions Form During Severe Bacteremic *Enterococcus faecalis* Infection

Armand O. Brown[1], Kavindra V. Singh[2], Melissa R. Cruz[1], Karan Gautam Kaval[1], Liezl E. Francisco[3], Barbara E. Murray[1,2], and Danielle A. Garsin[1*]

[1]Department of Microbiology and Molecular Genetics, The University of Texas Health Science Center at Houston, Houston TX, USA

[2] Division of Infectious Diseases, Department of Internal Medicine, The University of Texas Health Science Center at Houston, Houston, TX, USA

[3] Department of Biochemistry and Structural Biology, The University of Texas Health Science Center at San Antonio, San Antonio, TX, USA

*Corresponding author
Danielle.A.Garsin@uth.tmc.edu
713-500-5454

Running Title: Cardiac microlesions formed by *E. faecalis*

Abstract

Enterococcus faecalis is a significant cause of hospital-acquired bacteremia. Herein, the discovery is reported that cardiac microlesions form during severe bacteremic *E. faecalis* infection in mice. The cardiac microlesions were identical in appearance to those formed by *Streptococcus pneumoniae* during invasive pneumococcal disease (IPD). However, *E. faecalis* does not encode the virulence determinants implicated in pneumococcal microlesion formation. Rather, disulfide bond forming protein DsbA was found to be required for *E. faecalis* virulence in a *C. elegans* model and was necessary for efficient cardiac microlesion formation. Furthermore, *E. faecalis* promoted cardiomyocyte apoptotic and necroptotic cell death at sites of microlesion formation. Additionally, loss of DsbA caused an increase in pro-inflammatory cytokines unlike the wild-type strain, which suppressed the immune response. In conclusion, we establish that *E. faecalis* is capable of forming cardiac microlesions and identify features of both the bacterium and the host response that are mechanistically involved.

SUMMARY: This work presents the observation of cardiac microlesion formation during severe blood stream infection with *Enterococcus faecalis* in mice. Moreover, we identify the contribution of a novel enterococcal virulence determinant in modulating microlesion formation and the host immune response.

KEYWORDS: Enterococcus faecalis, cardiac, microlesions, sepsis, bacteremia, infection, virulence, thioredoxin, disulfide bond, necroptosis

ABSTRACT WORD COUNT: 149

TEXT WORD COUNT: 3,496

43 **Introduction**

44

45 *Enterococcus faecalis* is a Gram-positive bacterium that normally co-exists with the host as a
46 harmless commensal. However, it is capable of causing a variety of infections such as infective
47 endocarditis (IE), urinary tract infection (UTI), bacteremia, peritonitis, prosthetic joint infection, and
48 endophthalmitis. A common complication associated with enterococcal bacteremia is
49 endocarditis, an infection that has a 1-year mortality rate of approximately 29% despite antibiotic
50 therapy [1]. Enterococci are the third most common cause of endocarditis in North America [2]
51 and, in patients with this infection, heart failure has been observed to occur with increased
52 frequency [3-9]. Endocarditis only involves infection of the surfaces of the heart - the formation
53 of biofilms on heart valves and inner chambers that develop into complex masses called
54 vegetations [10]. *E. faecalis* invasion of the deeper myocardial tissue to cause cardiac
55 microlesions has not previously been described.

56

57 Interestingly, another Gram-positive pathogen, *Streptococcus pneumoniae,* was recently shown
58 to invade the heart tissue during invasive pneumococcal disease (IPD) [11]. Importantly,
59 pneumococcal microlesions were determined to be associated with altered cardiac
60 electrophysiology, heart failure and scar formation during convalescence, which is thought to
61 predispose individuals to major adverse cardiac events (MACE) [11, 12]. Furthermore, cardiac
62 microlesions form following vascular endothelial cell invasion into the myocardial tissue through
63 the interactions of pneumococcal Choline binding protein A (CbpA) and pneumococcal teichoic
64 acid associated phosphorylcholine (ChoP) with host laminin receptor (LR) and platelet activating
65 factor receptor (PAFr), respectively. Cardiomyocyte death is mediated by exposure to the
66 pneumococcal secreted cholesterol-dependent pore forming toxin, pneumolysin [11, 12], and
67 hydrogen peroxide [13, 14]. Since the original observation of pneumococcal microlesions in 2014,

68 similar observations were seen during blood stream infections with *Francisella tularensis* [15], and
69 *Mycobacterium avium* [16], however the mechanisms involved were not characterized.
70
71 In this report, we show that cardiac microlesions also form during invasive *E. faecalis* infection.
72 The observed cardiac microlesions were identical in appearance and size to those formed by *S.*
73 *pneumoniae*, were diffuse across the myocardium, and characterized by an absence of immune
74 cell infiltration and cell death by apoptosis and necroptosis. Furthermore, an enterococcal
75 determinant required for microlesion formation, DsbA, was identified. DsbA was additionally
76 shown to enhance cell death and promote suppression of the immune response during *E. faecalis*
77 infection of a cardiomyocyte cell line.

78 **Materials and Methods**

79

80 ***C. elegans* survival assay**

81 *E. faecalis* strains were tested in *C. elegans* for survival as previously described [17]. The data is
82 representative of 3 independent experiments. Nematode survival was plotted with the log-rank
83 (Mantel-Cox) method using Prism 7 statistical software (GraphPad).

84

85 **Bacterial strains and growth analysis**

86 All *E. faecalis* strains used in this project are listed in Table S1. For growth analysis, overnight
87 cultures were diluted to an OD_{600nm} of 0.05 in brain heart infusion (BHI) medium (Difco) or serum
88 [18, 19] in a volume of 200µl / well in a 96-well plate. The 96-well plate containing the diluted
89 cultures were placed in a prewarmed 37ºC BioTek Cytation 5 plate reader, and OD_{600nm}
90 measurements were taken every 10 minutes for 16 hours.

91

92 **Mouse peritonitis and cardiac microlesion model**

93 The mouse peritonitis model was performed as described previously [20]. The method for
94 identifying and evaluating cardiac microlesion formation was conducted as described previously
95 [11]. Briefly, female, ~4 – 6-week old (~25g), ICR outbred mice were obtained from Envigo
96 (Indianapolis, Indiana) and infected intraperitoneally with 3.8 - 4.2 $x10^8$ CFUs of *E. faecalis*. Mouse
97 hearts were harvested 24-48 hours post-infection at the point when the animals showed signs of
98 severe sepsis indicated by ruffled fur, labored breathing and little movement. The hearts were
99 formalin fixed and sent to The University of Texas Health Science Center Histopathology
100 Laboratory for paraffin embedding, sectioning, and hematoxylin and eosin H&E) staining. Paraffin
101 embedded mouse hearts were first bisected and sectioned longitudinally. 20 sections were cut
102 per block, and every 5th section H&E stained in order to measure the number and relative

103 distribution of the microlesions. Cardiac microlesions were averaged across sections, and the
104 differences between mouse groups compared using *Student's* two-tailed t-test. Experiments were
105 performed in accordance with protocols approved by the Animal Welfare Committee of the
106 University of Texas Health Science Center at Houston AWC-19-0058.
107
108 **Invasion assay**
109 SVEC4-10 Endothelial Cells (ATCC) were seeded in 24 well plates at a cell density of $1.5x10^5$
110 cells/ml. After 24 hours, the cells were washed three times with PBS and infected with *E. faecalis*
111 at a MOI of 10 for 4 hours in antibiotic free Dulbecco's Modified Eagle's Medium (ATCC). The
112 cells were then washed with Dulbecco's (1X) PBS three times, treated with trypsin, diluted in PBS,
113 and plated for quantification. To measure intracellular numbers of *E. faecalis*, cells that were
114 washed three times with Dulbecco's (1X) PBS 4 h.p.i., then treated with DMEM (ATCC)
115 supplemented with 15 µg/ml vancomycin and 150 µg/ml gentamicin. 24 hours later, the wells were
116 washed three times with Dulbecco's (1X) PBS, lysed using 0.1% Triton-X-100, and diluted and
117 plated for intracellular quantification. The ratio of invasion to attachment was used to calculate the
118 percent of invasion. The experiments were conducted on 3 independent occasions and were
119 performed using triplicate wells for each strain. Attachment and invasion values were averaged
120 from each experiment, and statistically analyzed using *Student's* two-tailed t-test.
121
122 **Cytotoxicity and inflammatory cytokine panel microtiter plate reader assay**
123 HL-1 cardiomyocytes were obtained from Sigma-Aldrich and SVEC4-10 Endothelial Cells were
124 obtained from ATCC. HL-1 cardiomyocytes (Sigma-Aldrich) were seeded into 24-well plates at a
125 concentration of $5x10^5$ cells/ml. 24 hours later, the cells were washed three times with Dulbecco's
126 (1X) PBS, and infected with *E. faecalis* at a MOI of 10 for 4 hours in antibiotic free Claycomb
127 medium. Supernatant was collected, and cytotoxicity assayed using CytoTox-ONE™

128 Homogeneous Membrane Integrity Assay Kit (Promega). For HL-1 infected cardiomyocytes,
129 inflammatory chemokines and cytokines were additionally analyzed using a Mouse Cytokine
130 ELISA Plate Array III Colorimetric Assay (Signosis). The data represent an average of at least 3
131 independent experiments for each strain and were analyzed using *Student's* two-tailed t-test.
132

133 **Immunofluorescence microscopy**

134 Immunofluorescence microscopy was conducted as described previously [11]. Briefly, paraffin
135 embedded sections were treated with 1:100 rabbit Anti-mouse MLKL (phospho S345) antibody
136 [EPR9515(2)] in order to detect phosphorylated MLKL (Abcam), and 1:100 rat anti-mouse MLKL
137 antibody (Millipore-Sigma) for MLKL detection followed by treatment with 1:1000 chicken anti-
138 rabbit IgG (H+L) cross-adsorbed secondary Alexa Fluor 594 antibody (ThermoFisher), and 1:1000
139 goat anti-rat IgG (H+L) secondary FITC antibody (ThermoFisher) respectively. A rabbit anti-
140 *Enterococcus faecalis* antibody (Abcam) was used at a concentration of 1:1000 to detect *E.*
141 *faecalis* followed by treatment with 1:1000 goat anti-rabbit IgG (H&L), FITC conjugated antibody
142 (Invitrogen). A rat anti-PARP (MAB600) antibody (R&DSystems) was used at a concentration of
143 1:100 followed by treatment with 1:1000 goat anti-rat IgG (H+L) cross-adsorbed secondary Alexa
144 Fluor 594 antibody (ThermoFisher) to detect PARP. All stained sections were counterstained with
145 1:1000 DAPI (ThermoFisher) and mounted with Hardset™ Antifade Mounting Medium.
146 Visualization of fluorescence was obtained using standard excitation and emission wavelengths
147 for Alexa 594, FITC, and DAPI on an Olympus FV3000RS high-speed, high-sensitivity, inverted
148 laser scanning confocal microscope.
149

150 **Generation of rabbit anti-DsbA antisera**

151 His-tagged recombinant DsbA was overexpressed in Rosetta-2(DE3) *E. coli* (Sigma-Aldrich) and
152 isolated by affinity purification via HisPur Nickel-NTA Resin (ThermoFisher) packed columns

153 followed by Fast Protein Liquid Chromatography (FPLC) to obtain highly pure samples of
154 recombinant DsbA. Cocalico Biologicals (Reamstown, PA) generated anti-DsbA antisera by
155 immunizing rabbits with the recombinant protein.
156

157 ***E. faecalis* whole cell lysate and Western blot**

158 A 5 ml culture of *E. faecalis* grown in BHI medium at 37ºC for 15-16 hours followed by a 1:10
159 dilution in 5 ml of fresh BHI. After 3.5 hours to achieve exponential growth, the culture was
160 centrifuged at 6,010 x G and the supernatant removed. The pellet was resuspended in 1ml of
161 buffer (10 mM Tris/HCl pH 7.5 and 200 mM NaCl) containing cOmplete™, EDTA-free Protease
162 Inhibitor Cocktail (Roche). Following sonication of the pellet on ice, the sample was centrifuged
163 at 10,000 x G for 5 minutes and supernatant collected for electrophoresis. Total protein in the
164 whole cell lysate was measured using the *DC* Protein Assay (BioRad). Following the loading of
165 10µg of cell lysate, electrophoresis and transfer of protein to a PVDF membrane, the membrane
166 was incubated overnight at 4ºC in a 5% milk solution containing a 1:1000 dilution of rabbit anti-
167 DsbA antisera followed by incubation with a Goat anti-rabbit IgG HRP (ThermoFisher) secondary
168 antibody at a dilution of 1:10,000 at room temperature for 30 minutes prior to development with a
169 chemiluminescent kit (ThermoFisher).

170 **Results**

171

172 **Cardiac microlesions form during severe bacteremic *E. faecalis* infection.** In previous work,
173 we implicated a previously uncharacterized *E. faecalis* thioredoxin known as DsbA (disulfide bond
174 forming protein A) as a requirement for the stability of EntV, a secreted bacteriocin that inhibits
175 hyphal morphogenesis of the human fungal pathogen *Candida albicans* [21, 22]. To test if these
176 proteins had any effects on the fitness and pathogenicity of *E. faecalis*, we infected
177 *Caenorhabditis elegans* with Δ*dsbA* and Δ*entV E. faecalis* mutants and measured survival. As
178 shown in Figure 1A, loss of *dsbA* significantly attenuated mortality in infected nematodes. Note
179 that the Δ*dsbA* mutant did not manifest different growth kinetics when grown in culture medium
180 compared to wild-type, ruling out a general growth defect (Figure S1A). Infection with the
181 complement, Δ*dsbA::dsbA*, partially rescued the Δ*dsbA* phenotype. The partial complementation
182 was attributed to the DsbA protein being produced at lower levels in the complemented strain
183 (Figure 1B and S2). No significant difference in nematode survival was observed following
184 infection with either the Δ*entV* mutant or its complement (Figure 1A). Considering that EntV is the
185 only known substrate of *E. faecalis* DsbA, the results suggest that DsbA has additional targets
186 that affect pathogenicity.

187

188 Based on these results, we wanted to know if loss of DsbA also affected virulence in a vertebrate
189 animal model of *E. faecalis* infection. Therefore, the mutants were tested in a mouse model in
190 which animals were injected intra-peritoneally with *E. faecalis* resulting in generalized bacteremia
191 leading to mortality. Significant survival differences between the mice infected with the different
192 strains were subtle, but significant attenuation by the *dsbA* mutant was observed when data from
193 three separate experiments were combined to generate an n close to 20 for each group (Figure
194 S3). To further study the contribution of *dsbA*, various organs were collected in order to determine

195 if *E. faecalis* infection induced any strain-specific, pathological effects. To our surprise, cardiac
196 microlesions were discovered within the myocardium that were devoid of immune cell infiltrate
197 regardless of which *E. faecalis* strain was used (Figures 2A, B and S4). The microlesions
198 appeared to form within roughly the same time frame (~24 h.p.i.) as cardiac microlesions that
199 have previously been reported to occur during invasive infection with *S. pneumoniae* [11].
200
201 To verify that the observed microlesions were the result of infection by *E. faecalis*,
202 immunofluorescent staining on paraffin embedded cardiac tissue sections from mice infected with
203 *E. faecalis* with a polyclonal anti-enterococcal IgG antibody was performed and revealed the
204 presence of dense aggregates of *E. faecalis* within the microlesions (Figure 2C). The presence of
205 bacterial DNA was further verified by counterstaining with DAPI, revealing an accumulation of
206 non-cardiomyocyte nuclear DNA within microlesions (Figure 2D). To determine the contribution
207 of DsbA, cardiac microlesions found on hematoxylin and eosin stained paraffin embedded cardiac
208 sections were quantified following infection with Δ*dsbA*. A significant attenuation in microlesion
209 formation during infection with Δ*dsbA* was observed relative to wild-type, while no significant
210 difference was observed in mice infected with the *dsbA* complement (Figure 2E). Furthermore,
211 when the sizes of the cardiac microlesions were compared, the wild-type lesions were significantly
212 larger than those found in the Δ*dsbA* infected mice (Figure 2F). Importantly, the size of the
213 microlesions appeared to correlate with level of *dsbA* expression observed in Western blots of *E.*
214 *faecalis* whole cell lysates (Figure 1B), with the Δ*dsbA*::*dsbA* strain manifesting an in-between
215 phenotype to that of the *ΔdsbA* and wild-type strains, consistent with partial complementation. It
216 is possible that less microlesion formation occurred with the Δ*dsbA* strain due poor growth in the
217 blood, but we do not favor this model as in vitro growth curves in serum showed no defect (Figure
218 S1B). In conclusion, these data demonstrate that cardiac microlesion formation occurs during
219 systematic infection with *E. faecalis* and is dependent on DsbA.

220

221 **Apoptosis and necroptosis contribute to cardiomyocyte cell death within microlesions.** In
222 previous studies of pneumococcal cardiac microlesion formation, apoptosis was found to be
223 associated with microlesion formation in mice [11]. A subsequent study determined that
224 cardiomyocyte cell death occurs following exposure to pneumolysin (*ply*) and pneumococcal
225 pyruvate oxidase (*spxB*) derived hydrogen peroxide [14]. Based on these observations and the
226 fact that *E. faecalis* lacks *ply* and *spxB* homologs, we sought to determine whether *E. faecalis*
227 could promote cell death of cardiomyocytes and identify the mechanism. To determine if apoptosis
228 contributes to *E. faecalis* microlesion formation, we performed immunofluorescent microscopy on
229 heart sections of infected mice to detect PARP [Poly(ADP-ribose) Polymerase], an enzyme that
230 is proteolytically cleaved by the effector Caspase-3, and is one hallmark event of apoptosis. In
231 agreement with previous reports, markers of apoptosis were observed to be concentrated at sites
232 of microlesion formation (Figure 3A and S5).

233

234 In addition to apoptosis, we hypothesized that necroptosis also contributes to *E. faecalis* mediated
235 cardiac microlesion formation. Necroptosis is a programmed form of necrotic cell death that is
236 generally inflammatory, and has been shown to contribute to the formation of *S. pneumoniae*
237 microlesions within the myocardium of acutely ill mice and non-human primates [12]. Importantly,
238 necroptosis is considered a key cell death pathway in cardiomyocytes during ischemia-
239 reperfusion injury and acute coronary syndrome [23-25]. To test the hypothesis that necroptosis
240 contributes to the formation of *E. faecalis* microlesions, we stained for markers of necroptosis [26],
241 such as mixed lineage kinase domain-like pseudokinase (MLKL) and phosphorylated MLKL, on
242 cardiac tissue sections obtained from infected mice. As a result, we detected concentrated signals
243 within the microlesions (Fig 3B and Figure S6) that suggest that necroptosis does indeed
244 contribute to *E. faecalis* cardiac microlesion formation.

245

246 To further look at the effects of *E. faecalis* and the *dsbA* mutant on heart cells, we infected HL-1
247 cardiomyocytes and subsequently measured lactate dehydrogenase (LDH) release into the cell
248 culture supernatant to assess cell death. As shown in Figure 3C, cell death of the cardiomyocytes
249 is significantly decreased following exposure to the *dsbA* mutant compared to wild-type
250 suggesting that DsbA contributes to cardiac cell death (Figure 3C). While *E. faecalis* promoted
251 death of the cardiomyocytes, antibiotic protection assays indicated that both the wild-type and
252 *dsbA* mutant bacteria were unable to invade cardiomyocytes relative to endothelial cells (Figure
253 3D). Taken together, these results suggest that during bacteremia, *E. faecalis* is able to
254 translocate across the vascular endothelium in order to enter the myocardial tissue. Once there,
255 *E. faecalis* is unable to invade cardiomyocytes, but can form microcolonies that promote
256 necroptosis in addition to apoptosis. Whether other cell death pathways additionally contribute
257 will be fodder for future investigations.

258 **Cardiomyocyte inflammatory cytokine response is suppressed following exposure to *E.***
259 ***faecalis*.** Cardiac microlesions are characterized by bacteria filled vacuoles that are largely devoid
260 of immune cell infiltrate [11, 27]. Previous efforts to explain the lack of an immune response to
261 pneumococcal microlesions have yielded interesting insights. For example, *S. pneumoniae* within
262 microlesions are thought to subvert the host response through a biofilm-mediated mechanism
263 involving the pneumolysin mediated killing of resident macrophages, thus creating a more
264 permissive environment for pneumococcal growth and survival [13]. There are also examples of
265 *E. faecalis* subverting the immune response. In previous work, it was shown that *E. faecalis* can
266 survive within mouse peritoneal macrophages for extended periods of time [28] and can also resist
267 phagosome acidification and autophagy [29]. Additionally, *E. faecalis* was shown to activate
268 Phosphatidylinositol 3-Kinase signaling that inhibits apoptosis [30]. Because *E. faecalis* does not
269 encode a pneumolysin homolog, nor does it secrete toxins known to kill macrophages or other

270 immune cells, we wanted to examine the immune response to *E. faecalis* within cardiomyocytes.
271 Therefore, following infection with *E. faecalis*, inflammatory chemokine and cytokine levels were
272 measured. Wild-type *E. faecalis* was discovered to promote an immune quiescent response, while
273 the *dsbA* mutant caused a more inflammatory immune response (Figure 4A and Table S2).
274 Specifically, infection of cardiomyocytes with wild-type increased the expression of two pro-
275 inflammatory cytokines IL-4 and b-NGF cytokines [31, 32]. Modest increases were also observed
276 in VEGF, an important determinant of sepsis morbidity and mortality [33], and GM-CSF that
277 serves as an immunomodulatory cytokine [34]. In contrast, cardiomyocytes infected with Δ*dsbA*
278 led to increases in Rantes, IFNr, MIP-1a, and IL-12, with modest increases also observed in Leptin
279 and G-CSF. With the exception of G-CSF, an immunomodulatory cytokine with roles in cardiac
280 cell generation and repair [35, 36], all of the other aforementioned cytokines are pro-inflammatory
281 [37-40]. These results implicate the contribution of specific host signaling pathways that are
282 normally suppressed in the presence of DsbA during infection, as modeled in Figure 4B.
283 Collectively, these data suggest that *E. faecalis* is capable of suppressing the host cardiomyocyte
284 immune response.

285 **Discussion**

286

287 In this work, we demonstrated for the first time that cardiac microlesions form during severe *E.*
288 *faecalis* bacteremic infection of mice. Importantly, microlesions occurred despite *E. faecalis* not
289 encoding homologs of the pneumococcal virulence determinants implicated in microlesion
290 formation. These data suggest that *E. faecalis* may be expressing functionally redundant proteins
291 that serve to promote similar interactions to *S. pneumoniae* in mediating microlesion formation,
292 such as CbpA and pneumolysin, which facilitate vascular endothelial cell translocation and
293 cardiomyocyte cell death, respectively. Indeed, while *E. faecalis* does not encode a CbpA
294 homolog, it does encode other proteins capable of binding host extracellular matrix proteins.
295 These include EfbA, which binds fibronectin [41], ACE, which binds laminin receptor [42], and Ebp
296 pili that bind fibrinogen [43].

297

298 Interestingly, we did discover one factor, DsbA, that contributes to microlesion formation and
299 inhibits the cardiomyocyte inflammatory immune response, as modeled in Figure 4B. Dsb proteins
300 work to catalyze disulfide bond formation in proteins and have been best studied in Gram-negative
301 bacteria [44, 45]. While Dsb proteins have established importance in the biology of certain Gram-
302 positive bacteria, Dsb proteins are not well studied in Firmicutes like *E. faecalis* and have generally
303 not been considered important [44]. Most of these species secrete few proteins containing
304 cysteines and some, notably *S. pneumoniae*, do not encode any thiol-disulfide oxidoreductases
305 [46, 47]. Thus, it will be of interest to further investigate the role of Dsb proteins in these species.

306

307 Our prior work established EntV as a DsbA substrate, currently the only one identified [21].
308 However, loss of EntV did not reduce pathogenicity in the worm model (Figure 1A), and exposure
309 to EntV, even at very high concentrations, was non-toxic to mammalian cells [22]. As such, we do

310 not favor EntV as being the source of DsbA's effects. While the specific *E. faecalis* proteins
311 involved in modulating the host immune response are unknown, we speculate that the
312 Fibronectin-binding protein (Efb) and Choline binding protein may contribute to cardiac
313 microlesion formation by serving as functionally redundant proteins to pneumococcal CbpA, a
314 virulence determinant known to be integral to microlesion formation [11]. Moreover, both proteins
315 contain 5 cysteines and are expressed extracellularly. Thus, our future research efforts will be
316 geared toward identifying additional substrates of DsbA and to determining their contribution to
317 microlesion formation.
318
319 Pneumococcal ChoP interactions with host PAFr were determined to be a prerequisite for
320 vascular endothelial cell invasion during IPD. In light of our observations of *E. faecalis* invasion of
321 vascular endothelial cells despite an absence of this wall teichoic acid structure, it is possible that
322 another host receptor is required for endothelial cell invasion. Interestingly, recent studies focused
323 on bacterial cell wall entry and signaling in eukaryotic cells have identified a PAFr-independent
324 mechanism of tissue invasion that is actin-dependent and engenders Rac1, Cdc42, and
325 phosphatidylinositol 3-kinase (PI3K) signaling leading to cell wall internalization via a
326 macropinoctytosis-like pathway [48]. Whether such a pathway contributes to microlesion
327 formation is unknown. In the future, it will be of interest to study the mechanisms of tissue invasion
328 and the host signaling pathways involved.
329
330 Although the role of cardiac microlesion formation in humans during invasive disease remains
331 unclear, cardiac microlesion formation is becoming increasingly appreciated as a risk factor [49].
332 To our knowledge, no one has investigated whether cardiac microlesions form in humans during
333 enterococcal infection. We speculate that formation occurs and contributes to cardiac
334 abnormalities or death in patients with enterococcal infective endocarditis or sepsis [1, 3-9]. This

335 study builds on our understanding of cardiac microlesions by establishing *E. faecalis* as another
336 etiological agent capable of causing them in a vertebrate animal model. Considering that *E.*
337 *faecalis* microlesion pathology appears identical to that caused by *S. pneumoniae*, it is likely that
338 scar formation occurs following resolution of infection, potentially predisposing individuals to future
339 adverse cardiac events [11]. Taken together, these data highlight the need for further investigation
340 in order to understand the impact of microlesion formation on the heart and mortality during
341 invasive *E. faecalis* infection.

342 **Table S1. Strains used in this study**
343

***Enterococcus faecalis* Strains**				
Strain	**Genotype**	**Characteristics**	**Parent**	**Source**
OG1RF	Wild-type	Gel^+ Spr^+ Rf^R Fa^R	OG1	[50]
AOBD1	Δ*dsbA*	Gel^+ Spr^+ Rf^R Fa^R	OG1	[21]
AOBD2	Δ*dsbA::dsbA*	Gel^+ Spr^+ Rf^R Fa^R	OG1	[21]

344
345
346
347 **Table S2. Cytokine Profiling Expression Data**
348
349

Cytokine Profiling - Fold Change Data for 3 independent Experiments
4 hour infection with an MOI=10

	Exp. 1	Exp. 2	Exp. 3		
	OG1RF	OG1RF	OG1RF	Average	Std. Dev
TNF-a	-7%	7%	-2%	-1%	7%
IGF-1	2%	-7%	4%	0%	6%
VEGF	23%	4%	-2%	8%	13%
IL-6	7%	5%	1%	4%	3%
FGFb	11%	-28%	0%	-5%	20%
IFNr	5%	3%	-11%	-1%	9%
EGF	-10%	33%	2%	8%	23%
Leptin	0%	-16%	-1%	-6%	9%
IL-1a	-7%	-14%	4%	-6%	9%
IL-1b	-8%	-22%	18%	-4%	20%
G-CSF	1%	-22%	2%	-6%	14%
GM-CSF	-10%	19%	14%	7%	16%
MCP-1	-7%	-8%	11%	-1%	11%
M1P-1a	3%	3%	-17%	-4%	12%
SCF	-15%	5%	-3%	-5%	10%
Rantes	-13%	19%	-7%	0%	17%
PDGF-BB	-16%	8%	7%	0%	13%
b-NGF	-20%	12%	17%	3%	20%
IL-17a	-22%	-4%	9%	-5%	16%
IL-2	-9%	-10%	-5%	-8%	3%
IL-4	12%	-1%	9%	7%	7%
IL-10	11%	-13%	-3%	-2%	12%
Resistin	-13%	-3%	-6%	-8%	5%
IL-12	-3%	0%	-17%	-7%	9%
CCL11	-9%	-25%	3%	-10%	14%
CCL21	-17%	0%	-5%	-7%	9%
IL-3	8%	3%	5%	5%	2%
IL-13	-7%	-7%	10%	-1%	10%
IL-21	-24%	-14%	1%	-12%	13%
IL-22	-18%	-19%	-12%	-16%	4%
CXCL10	-12%	-10%	2%	-7%	8%
CXCL1	-5%	-4%	-13%	-7%	5%

*OG1RF ordered from Largest to smallest

	OG1RF	Δ*dsbA*
EGF	8%	3%
VEGF	8%	1%
GM-CSF	7%	1%
IL-4	7%	-12%
IL-3	5%	-1%
IL-6	4%	2%
b-NGF	3%	-8%
PDGF-BB	0%	-2%
IGF-1	0%	-6%
Rantes	0%	4%
TNF-a	-1%	-2%
IFNr	-1%	4%
IL-13	-1%	-3%
MCP-1	-1%	-2%
IL-10	-2%	-2%
M1P-1a	-4%	3%
IL-1b	-4%	-13%
SCF	-5%	-7%
FGFb	-5%	-8%
IL-17a	-5%	-14%
IL-1a	-6%	-7%
Leptin	-6%	0%
G-CSF	-6%	2%
CXCL10	-7%	-11%
IL-12	-7%	1%
CXCL1	-7%	-3%
CCL21	-7%	-9%
Resistin	-8%	-10%
IL-2	-8%	-11%
CCL11	-10%	-12%
IL-21	-12%	-9%
IL-22	-16%	-5%

	Exp. 1	Exp. 2	Exp. 3		
	Δ*dsbA*	Δ*dsbA*	Δ*dsbA*	Average	Std. Dev
TNF-a	-2%	5%	-8%	-2%	6%
IGF-1	-15%	-7%	3%	-6%	9%
VEGF	2%	1%	0%	1%	1%
IL-6	0%	13%	-8%	2%	10%
FGFb	-7%	-15%	-2%	-8%	7%
IFNr	16%	7%	-12%	4%	14%
EGF	-8%	31%	-12%	3%	24%
Leptin	13%	-8%	-4%	0%	11%
IL-1a	-17%	-10%	7%	-7%	12%
IL-1b	-20%	-19%	-1%	-13%	11%
G-CSF	-12%	14%	3%	2%	13%
GM-CSF	-18%	18%	2%	1%	18%
MCP-1	-20%	-9%	23%	-2%	22%
M1P-1a	-6%	3%	13%	3%	10%
SCF	-10%	-20%	10%	-7%	15%
Rantes	-3%	20%	-4%	4%	14%
PDGF-BB	-23%	15%	4%	-2%	20%
b-NGF	-16%	-10%	1%	-8%	9%
IL-17a	-45%	-1%	4%	-14%	27%
IL-2	-35%	-1%	1%	-11%	20%
IL-4	-17%	-21%	2%	-12%	13%
IL-10	0%	-2%	-4%	-2%	2%
Resistin	-19%	-6%	-6%	-10%	7%
IL-12	-13%	14%	1%	1%	14%
CCL11	-13%	-30%	7%	-12%	18%
CCL21	-33%	4%	3%	-9%	21%
IL-3	-8%	2%	3%	-1%	6%
IL-13	-25%	-3%	19%	-3%	22%
IL-21	-23%	-10%	6%	-9%	15%
IL-22	-26%	-7%	18%	-5%	22%
CXCL10	-14%	-17%	-2%	-11%	8%
CXCL1	-12%	-15%	17%	-3%	17%

351
352 **Figure Legends**
353

354 **Figure 1. *dsbA* deficient *E. faecalis* show reduced virulence in a *C. elegans* survival assay**.
355 **(A)** L4 stage *C. elegans* were infected with *E. faecalis*. This figure is representative of 3
356 independent experiments with 30 worms/group. ****Asterisks indicate a $P < 0.0001$, ** a $P < 0.01$
357 when compared to OG1RF following pairwise analysis by log-rank (Mantel-Cox). **(B)** Western blot
358 performed by SDS-PAGE separation of *E. faecalis* whole cell lysates followed by hybridization of
359 DsbA using rabbit anti-DsbA antisera. Equal loading is ensured by visualization of a non-specific
360 band at 40 kDa. Image is representative of 3 independent Western blot experiments.
361

362 **Figure 2. Cardiac microlesions form during invasive *E. faecalis* infection and are**
363 **attenuated by loss of *dsbA***. Cardiac microlesions were observed using light microscopy of
364 hematoxylin and eosin (H&E) stained paraffin embedded cardiac sections at 40X magnification
365 **(A)**, and 100X magnification **(B)**. Immunofluorescent detection of wild-type *E. faecalis* was imaged
366 using a 20X objective at 3X zoom (total of 60X magnification), a FITC conjugated anti-
367 enterococcal antibody **(C)**, and DAPI for DNA staining **(D)**. Total microlesion counts **(E)**, and size
368 measurements **(F)**, were obtained by quantification using light microscopy of H&E stained paraffin
369 embedded cardiac sections from mice infected for 24-48 hours with *E. faecalis* (OG1RF n=14,
370 Δ*dsbA* n=14, Δ*dsbA*::*dsbA* n=14). The data were averaged from 3 independent experiments and
371 analyzed using *Student's* two-tailed t-test (* indicate a $P < 0.05$, ** $P < 0.01$, *** a $P < 0.001$).
372

373 **Figure 3. Necroptosis contributes to cardiotoxicity within cardiac microlesions**. **(A)**
374 Immunofluorescent microscopy of paraffin embedded cardiac cross sections at 20X were
375 performed to detect *E. faecalis* using FITC conjugated anti-faecalis antibodies, and apoptosis
376 using Alexa 594 conjugated anti-PARP antibodies at sites of microlesion formation, while DAPI

377 was used to stain nuclei. **(B)** Immunofluorescent microscopy of paraffin embedded cardiac cross
378 sections at 20X were performed to detect MLKL using FITC conjugated anti-MLKL antibodies, and
379 Alexa 594 conjugated anti-phosphorylated MLKL antibodies at sites of microlesion formation,
380 while DAPI was used to stain nuclei. **(C)** *E. faecalis* induced cell death in HL-1 cardiomyocytes 4
381 hours post-infection (h.p.i.) as determined by measuring lactate dehydrogenase. The data
382 represent an average of 3 independent experiments and were analyzed using *Student's* two-tailed
383 t-test (* indicate a $P < 0.05$). **(D)** Comparison of OG1RF and Δ*dsbA* invasion rates into HL-1
384 cardiomyocytes and SVEC endothelial cells. The graph represents data from 3 independent
385 experiments that were analyzed using *Student's* two-tailed t-test.
386
387 **Figure 4. Wild-type *E. faecalis* suppresses the cardiomyocyte inflammatory response *in-***
388 ***vitro*. (A)** HL-1 cardiomyocytes exposed to *E. faecalis* promote a suppressed inflammatory
389 response while Δ*dsbA* infected cardiomyocytes yield a more inflammatory response. Data was
390 obtained from the fold-expression change analysis (relative to uninfected controls) of at least 3
391 independent experiments for each strain. **(B)** Model of *E. faecalis* mediated suppression of the
392 host cardiomyocyte immune response and effect on microlesion size. Wild-type *E. faecalis* is
393 postulated to downregulate the cardiomyocyte immune response more effectively than the *dsbA*
394 mutant resulting in more cell death and increased lesion size. However, both strains cause cell
395 death by apoptosis and necroptosis and inhibit immune cell infiltration.
396
397 **Supplemental Figure 1. *E. faecalis* growth curve. (A)** *E. faecalis* strains were grown for 15
398 hours in BHI and absorbance (OD_{600nm}) measured every 10 minutes for 16 hours. **(B)** *E. faecalis*
399 grown in serum and absorbance (OD_{600nm}) measured every 10 minutes for 16 hours. Figures are
400 representative of 3 independent experiments.
401

402 **Supplemental Figure 2. Coomassie stained SDS-PAGE gel of *E. faecalis* whole cell lysates**
403 **separated by electrophoresis. (A)** SDS-PAGE separation of *E. faecalis* whole cell lysates was
404 stained with Coomassie to verify that each well received 10 µg / lane of whole cell lysate.
405 Coomassie stained gel is the loading control for the Western blot in Figure 1B.
406
407 **Supplemental Figure 3. DsbA is required for *E. faecalis* pathogenesis. (A)** Mice (n=17-20)
408 challenged with 3.8 – 4.2 x 10^8 CFUs of *E. faecalis* in a mouse model of peritonitis were assessed
409 for survival over 96 hours. Mice infected with Δ*dsbA E. faecalis* lived significantly longer (P =
410 0.0051) than mice challenged with wild-type or the complemented strain (no significant
411 difference). Survival curve was calculated from 3 independent experiments using log-rank
412 analysis.
413
414 **Supplemental Figure 4. (A)** 40X magnification image of cardiac microlesion formation in mice
415 infected with Δ*dsbA.* **(B)** 100X image of cardiac microlesion in Figure S4A. **(C)** 40X magnification
416 image of cardiac microlesion formation in mice infected with Δ*dsbA*::*dsbA*. **(D)** 100X image of
417 cardiac microlesion in Figure S4C.
418
419 **Supplemental Figure 5. Necroptosis contributes to cardiotoxicity within cardiac**
420 **microlesions**. **(A)** Immunofluorescent microscopy of paraffin embedded cardiac cross sections
421 using a 20X objective at 4X Zoom (80X total magnification) were performed to detect MLKL using
422 FITC conjugated anti-MLKL antibodies, and Alexa 594 conjugated anti-phosphorylated MLKL
423 antibodies at sites of microlesion formation, while DAPI was used to stain nuclei.
424
425 **Supplemental Figure 6. Apoptosis contributes to cell death within cardiac microlesions**.
426 **(A)** Immunofluorescent microscopy of paraffin embedded cardiac cross sections using a 20X

427 objective at 4X Zoom (80X total magnification) were performed to detect *E. faecalis* using FITC
428 conjugated anti-*E. faecalis* antibodies, and Alexa 594 conjugated anti-PARP antibodies at sites of
429 microlesion formation, while DAPI was used to stain nuclei.
430
431
432 References
433
434 1. Chirouze C, Athan E, Alla F, et al. Enterococcal endocarditis in the beginning of the 21st
435 century: analysis from the International Collaboration on Endocarditis-Prospective Cohort Study.
436 Clin Microbiol Infect 2013; 19:1140-7.
437 2. Agudelo Higuita NI, Huycke MM. Enterococcal Disease, Epidemiology, and Implications for
438 Treatment. In: Gilmore MS, Clewell DB, Ike Y, Shankar N, eds. Enterococci: From Commensals
439 to Leading Causes of Drug Resistant Infection. Boston, 2014.
440 3. Cabell CH, Jollis JG, Peterson GE, et al. Changing patient characteristics and the effect on
441 mortality in endocarditis. Arch Intern Med 2002; 162:90-4.
442 4. Garvey GJ, Neu HC. Infective endocarditis--an evolving disease. A review of endocarditis at
443 the Columbia-Presbyterian Medical Center, 1968-1973. Medicine (Baltimore) 1978; 57:105-27.
444 5. Geraci JE, Martin WJ. Antibiotic therapy of bacterial endocarditis. VI. Subacute enterococcal
445 endocarditis; clinical, pathologic and therapeutic consideration of 33 cases. Circulation 1954;
446 10:173-94.
447 6. Jawetz E, Sonne M. Penicillin-streptomycin treatment of enterococcal endocarditis. A re-
448 evaluation. N Engl J Med 1966; 274:710-5.
449 7. Lerner PI, Weinstein L. Infective endocarditis in the antibiotic era. N Engl J Med 1966; 274:388-
450 93 concl.

451 8. Olaison L, Schadewitz K, Swedish Society of Infectious Diseases Quality Assurance Study
452 Group for E. Enterococcal endocarditis in Sweden, 1995-1999: can shorter therapy with
453 aminoglycosides be used? Clin Infect Dis 2002; 34:159-66.
454 9. Pelletier LL, Jr., Petersdorf RG. Infective endocarditis: a review of 125 cases from the University
455 of Washington Hospitals, 1963-72. Medicine (Baltimore) 1977; 56:287-313.
456 10. Garsin DA, Frank KL, Silanpaa J, et al. Pathogenesis and Models of Enterococcal Infection.
457 In: Gilmore MS, Clewell DB, Ike Y, Shankar N, eds. Enterococci: From Commensals to Leading
458 Causes of Drug Resistant Infection. Boston, 2014.
459 11. Brown AO, Mann B, Gao G, et al. Streptococcus pneumoniae translocates into the
460 myocardium and forms unique microlesions that disrupt cardiac function. PLoS Pathog 2014;
461 10:e1004383.
462 12. Reyes LF, Restrepo MI, Hinojosa CA, et al. Severe Pneumococcal Pneumonia Causes Acute
463 Cardiac Toxicity and Subsequent Cardiac Remodeling. Am J Respir Crit Care Med 2017;
464 196:609-20.
465 13. Shenoy AT, Brissac T, Gilley RP, et al. Streptococcus pneumoniae in the heart subvert the
466 host response through biofilm-mediated resident macrophage killing. PLoS Pathog 2017;
467 13:e1006582.
468 14. Brissac T, Shenoy AT, Patterson LA, Orihuela CJ. Cell Invasion and Pyruvate Oxidase-
469 Derived H2O2 Are Critical for Streptococcus pneumoniae-Mediated Cardiomyocyte Killing. Infect
470 Immun 2018; 86.
471 15. Makara MA, Hoang KV, Ganesan LP, et al. Cardiac Electrical and Structural Changes During
472 Bacterial Infection: An Instructive Model to Study Cardiac Dysfunction in Sepsis. J Am Heart
473 Assoc 2016; 5.
474 16. Headley CA, Gerberick A, Mehta S, et al. Nontuberculous mycobacterium M. avium infection
475 predisposes aged mice to cardiac abnormalities and inflammation. Aging Cell 2019; 18:e12926.

476 17. Garsin DA, Sifri CD, Mylonakis E, et al. A simple model host for identifying Gram-positive
477 virulence factors. Proc Natl Acad Sci U S A 2001; 98:10892-7.
478 18. Nallapareddy SR, Murray BE. Role played by serum, a biological cue, in the adherence of
479 Enterococcus faecalis to extracellular matrix proteins, collagen, fibrinogen, and fibronectin. J
480 Infect Dis 2008; 197:1728-36.
481 19. Teng F, Singh KV, Bourgogne A, Zeng J, Murray BE. Further characterization of the epa gene
482 cluster and Epa polysaccharides of Enterococcus faecalis. Infect Immun 2009; 77:3759-67.
483 20. Singh KV, Qin X, Weinstock GM, Murray BE. Generation and testing of mutants of
484 Enterococcus faecalis in a mouse peritonitis model. J Infect Dis 1998; 178:1416-20.
485 21. Armand O. Brown CEG, Melissa R. Cruz, Michael C. Lorenz, Danielle A. Garsin. Antifungal
486 activity of the Enterococcus faecalis peptide EntV requires protease cleavage and disulfide bond
487 formation. Mbio 2019; 10:1-13.
488 22. Graham CE, Cruz MR, Garsin DA, Lorenz MC. Enterococcus faecalis bacteriocin EntV inhibits
489 hyphal morphogenesis, biofilm formation, and virulence of Candida albicans. Proc Natl Acad Sci
490 U S A 2017; 114:4507-12.
491 23. Zhang T, Zhang Y, Cui M, et al. CaMKII is a RIP3 substrate mediating ischemia- and oxidative
492 stress-induced myocardial necroptosis. Nat Med 2016; 22:175-82.
493 24. Linkermann A, Hackl MJ, Kunzendorf U, Walczak H, Krautwald S, Jevnikar AM. Necroptosis
494 in immunity and ischemia-reperfusion injury. Am J Transplant 2013; 13:2797-804.
495 25. Linkermann A, Brasen JH, Darding M, et al. Two independent pathways of regulated necrosis
496 mediate ischemia-reperfusion injury. Proc Natl Acad Sci U S A 2013; 110:12024-9.
497 26. Kitur K, Wachtel S, Brown A, et al. Necroptosis Promotes Staphylococcus aureus Clearance
498 by Inhibiting Excessive Inflammatory Signaling. Cell Rep 2016; 16:2219-30.

499 27. Gilley RP, Gonzalez-Juarbe N, Shenoy AT, et al. Infiltrated Macrophages Die of Pneumolysin-
500 Mediated Necroptosis following Pneumococcal Myocardial Invasion. Infect Immun 2016; 84:1457-
501 69.
502 28. Gentry-Weeks CR, Karkhoff-Schweizer R, Pikis A, Estay M, Keith JM. Survival of
503 Enterococcus faecalis in mouse peritoneal macrophages. Infect Immun 1999; 67:2160-5.
504 29. Zou J, Shankar N. The opportunistic pathogen Enterococcus faecalis resists phagosome
505 acidification and autophagy to promote intracellular survival in macrophages. Cell Microbiol 2016;
506 18:831-43.
507 30. Zou J, Shankar N. Enterococcus faecalis infection activates phosphatidylinositol 3-kinase
508 signaling to block apoptotic cell death in macrophages. Infect Immun 2014; 82:5132-42.
509 31. Huang XL, Wang YJ, Yan JW, et al. Role of anti-inflammatory cytokines IL-4 and IL-13 in
510 systemic sclerosis. Inflamm Res 2015; 64:151-9.
511 32. Minnone G, De Benedetti F, Bracci-Laudiero L. NGF and Its Receptors in the Regulation of
512 Inflammatory Response. Int J Mol Sci 2017; 18.
513 33. Yano K, Liaw PC, Mullington JM, et al. Vascular endothelial growth factor is an important
514 determinant of sepsis morbidity and mortality. J Exp Med 2006; 203:1447-58.
515 34. Bhattacharya P, Thiruppathi M, Elshabrawy HA, Alharshawi K, Kumar P, Prabhakar BS. GM-
516 CSF: An immune modulatory cytokine that can suppress autoimmunity. Cytokine 2015; 75:261-
517 71.
518 35. Shimoji K, Yuasa S, Onizuka T, et al. G-CSF promotes the proliferation of developing
519 cardiomyocytes in vivo and in derivation from ESCs and iPSCs. Cell Stem Cell 2010; 6:227-37.
520 36. Martins A, Han J, Kim SO. The multifaceted effects of granulocyte colony-stimulating factor in
521 immunomodulation and potential roles in intestinal immune homeostasis. IUBMB Life 2010;
522 62:611-7.

523 37. Lee SH, Kwon JY, Kim SY, Jung K, Cho ML. Interferon-gamma regulates inflammatory cell
524 death by targeting necroptosis in experimental autoimmune arthritis. Sci Rep 2017; 7:10133.
525 38. Kothapalli R, Nyland SB, Kusmartseva I, Bailey RD, McKeown TM, Loughran TP, Jr.
526 Constitutive production of proinflammatory cytokines RANTES, MIP-1beta and IL-18
527 characterizes LGL leukemia. Int J Oncol 2005; 26:529-35.
528 39. La Cava A. Leptin in inflammation and autoimmunity. Cytokine 2017; 98:51-8.
529 40. Trinchieri G. Interleukin-12: a proinflammatory cytokine with immunoregulatory functions that
530 bridge innate resistance and antigen-specific adaptive immunity. Annu Rev Immunol 1995;
531 13:251-76.
532 41. Singh KV, La Rosa SL, Somarajan SR, Roh JH, Murray BE. The fibronectin-binding protein
533 EfbA contributes to pathogenesis and protects against infective endocarditis caused by
534 Enterococcus faecalis. Infect Immun 2015; 83:4487-94.
535 42. Nallapareddy SR, Qin X, Weinstock GM, Hook M, Murray BE. Enterococcus faecalis adhesin,
536 ace, mediates attachment to extracellular matrix proteins collagen type IV and laminin as well as
537 collagen type I. Infect Immun 2000; 68:5218-24.
538 43. .Nallapareddy SR, Singh KV, Sillanpaa J, et al. Endocarditis and biofilm-associated pili of
539 Enterococcus faecalis. J Clin Invest 2006; 116:2799-807.
540 44. Reardon-Robinson ME, Ton-That H. Disulfide-Bond-Forming Pathways in Gram-Positive
541 Bacteria. J Bacteriol 2015; 198:746-54.
542 45. Landeta C, Boyd D, Beckwith J. Disulfide bond formation in prokaryotes. Nat Microbiol 2018;
543 3:270-80.
544 46. Daniels R, Mellroth P, Bernsel A, et al. Disulfide bond formation and cysteine exclusion in
545 gram-positive bacteria. J Biol Chem 2010; 285:3300-9.

546 47. Dutton RJ, Boyd D, Berkmen M, Beckwith J. Bacterial species exhibit diversity in their
547 mechanisms and capacity for protein disulfide bond formation. Proc Natl Acad Sci U S A 2008;
548 105:11933-8.
549 48. Loh LN, Gao G, Tuomanen EI. Dissecting Bacterial Cell Wall Entry and Signaling in Eukaryotic
550 Cells: an Actin-Dependent Pathway Parallels Platelet-Activating Factor Receptor-Mediated
551 Endocytosis. MBio 2017; 8.
552 49. Musher DM, Abers MS, Corrales-Medina VF. Acute Infection and Myocardial Infarction. N
553 Engl J Med 2019; 380:171-6.
554 50. Murray BE, Singh KV, Ross RP, Heath JD, Dunny GM, Weinstock GM. Generation of
555 restriction map of Enterococcus faecalis OG1 and investigation of growth requirements and
556 regions encoding biosynthetic function. J Bacteriol 1993; 175:5216-23.
557

558 **FOOTNOTE PAGE**

559 **Conflict of Interest statement**

560 There are no conflicts of interest.

561 **Funding statement**

562 This work was supported by the National Institute of Dental and Craniofacial Research of the
563 National Institutes of Health under [grant number R01DE027608 to D. A. G.] and [grant number
564 F32DE027580 to A. O. B.]

565 **Meetings**

566 This work has not been presented.

567 **Corresponding author contact information**

568 Danielle A. Garsin, Ph.D.

569 6431 Fannin St.

570 MSB 1.168

571 Houston, TX 77030

572 Telephone: (713) 500-5454

573 Fax: (713) 500-5499

574 Email: Danielle.A.Garsin@uth.tmc.edu

575

Figure 1

A.

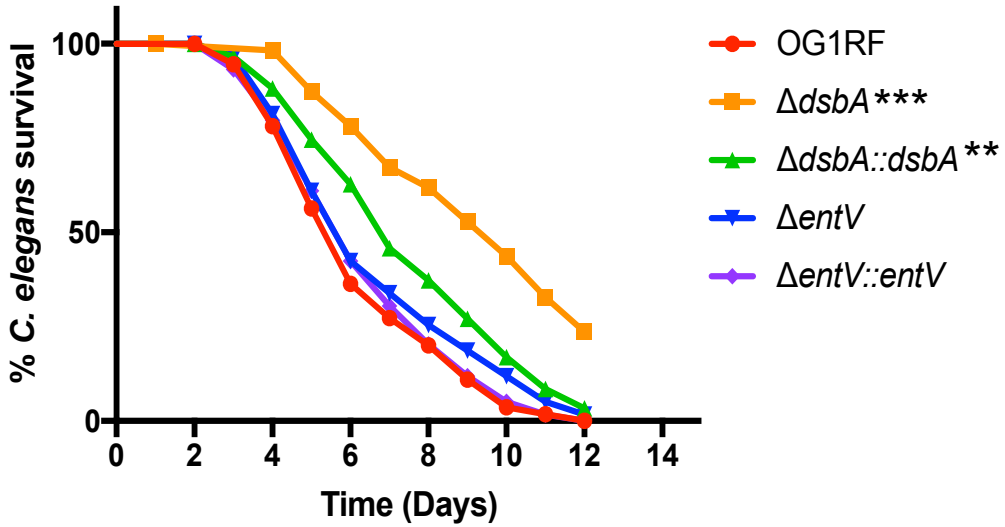
% C. elegans survival
100
50
0
0
2
4
6
8
10
12
14
Time (Days)
OG1RF
ΔdsbA***
ΔdsbA::dsbA**
ΔentV
ΔentV::entV

B.

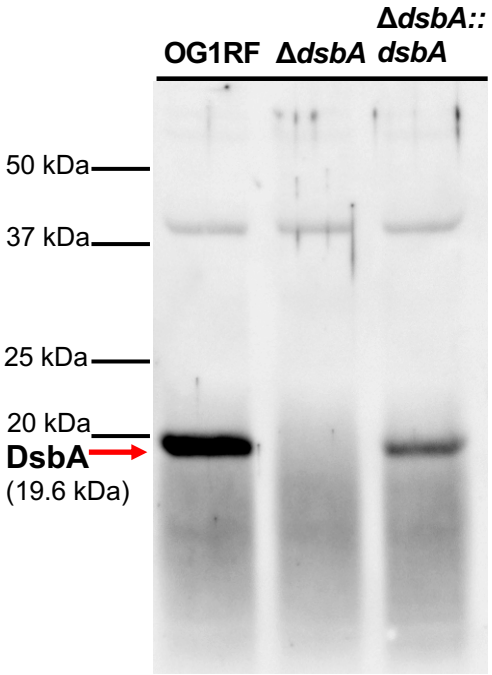
OG1RF
ΔdsbA
ΔdsbA::
dsbA
50 kDa
37 kDa
25 kDa
20 kDa
DsbA
(19.6 kDa)

Figure 2

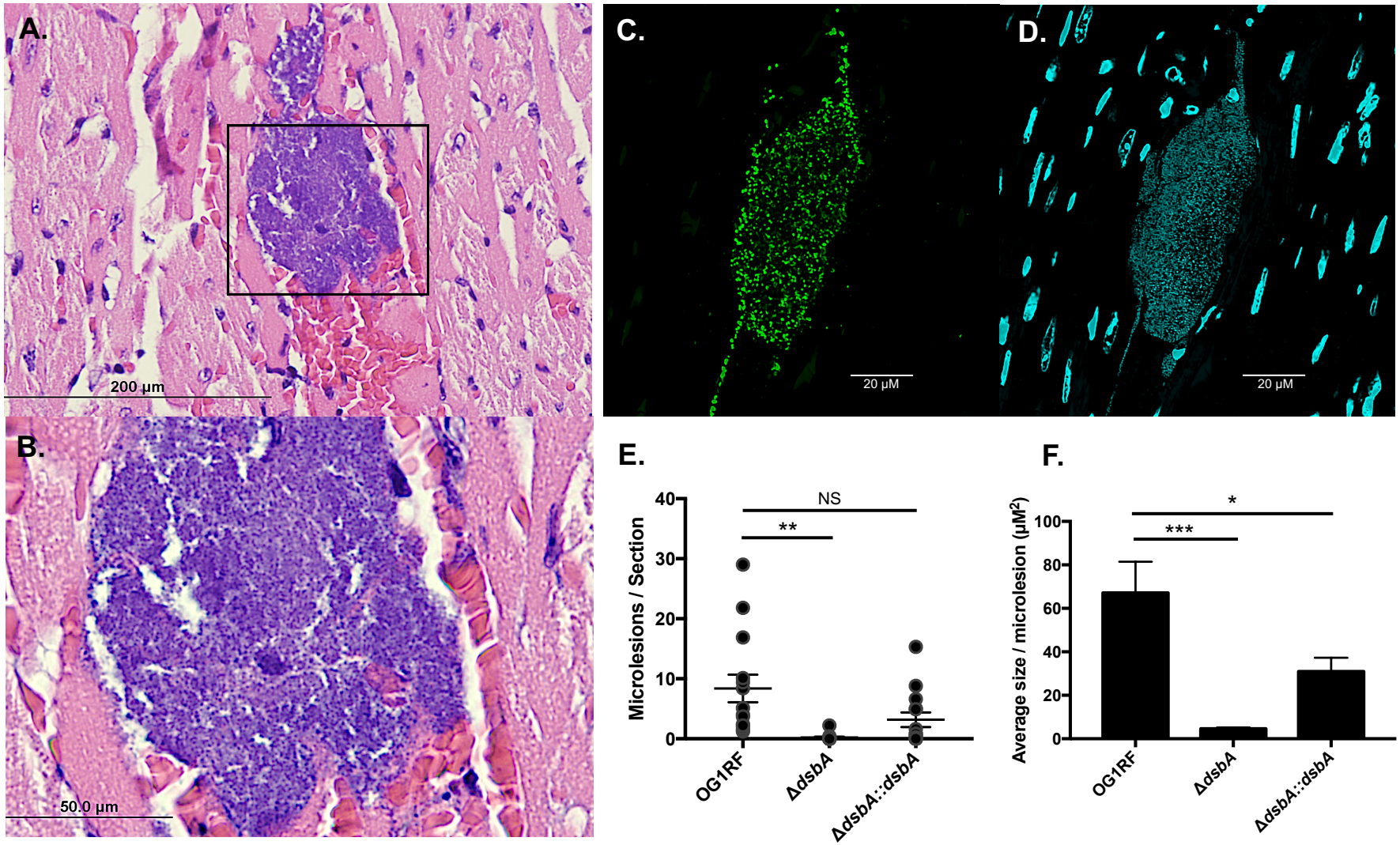
A.
200 µm
B.
50.0 µm
C.
20 µM
D.
20 µM
E.
Microlesions / Section
40
30
20
10
0
NS
**
OG1RF
ΔdsbA
ΔdsbA::dsbA
F.
Average size / microlesion (µM²)
100
80
60
40
20
0
*
***
OG1RF
ΔdsbA
ΔdsbA::dsbA

Figure 3

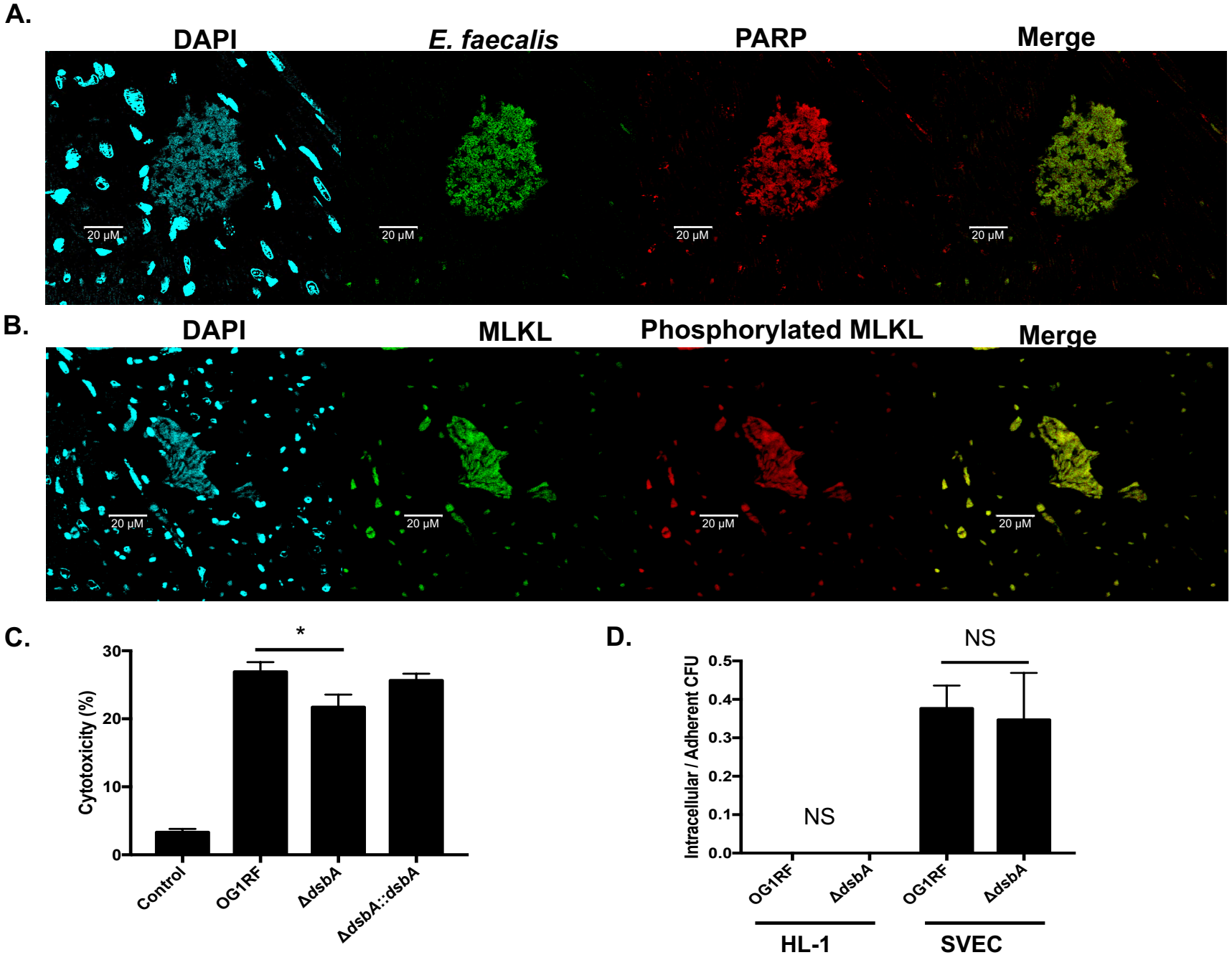
A.
DAPI
E. faecalis
PARP
Merge
20 µM
B.
DAPI
MLKL
Phosphorylated MLKL
Merge
20 µM
C.
*
Cytotoxicity (%)
30
20
10
0
Control
OG1RF
ΔdsbA
ΔdsbA::dsbA
D.
NS
NS
Intracellular / Adherent CFU
0.5
0.4
0.3
0.2
0.1
0.0
OG1RF
ΔdsbA
OG1RF
ΔdsbA
HL-1
SVEC

Figure 4

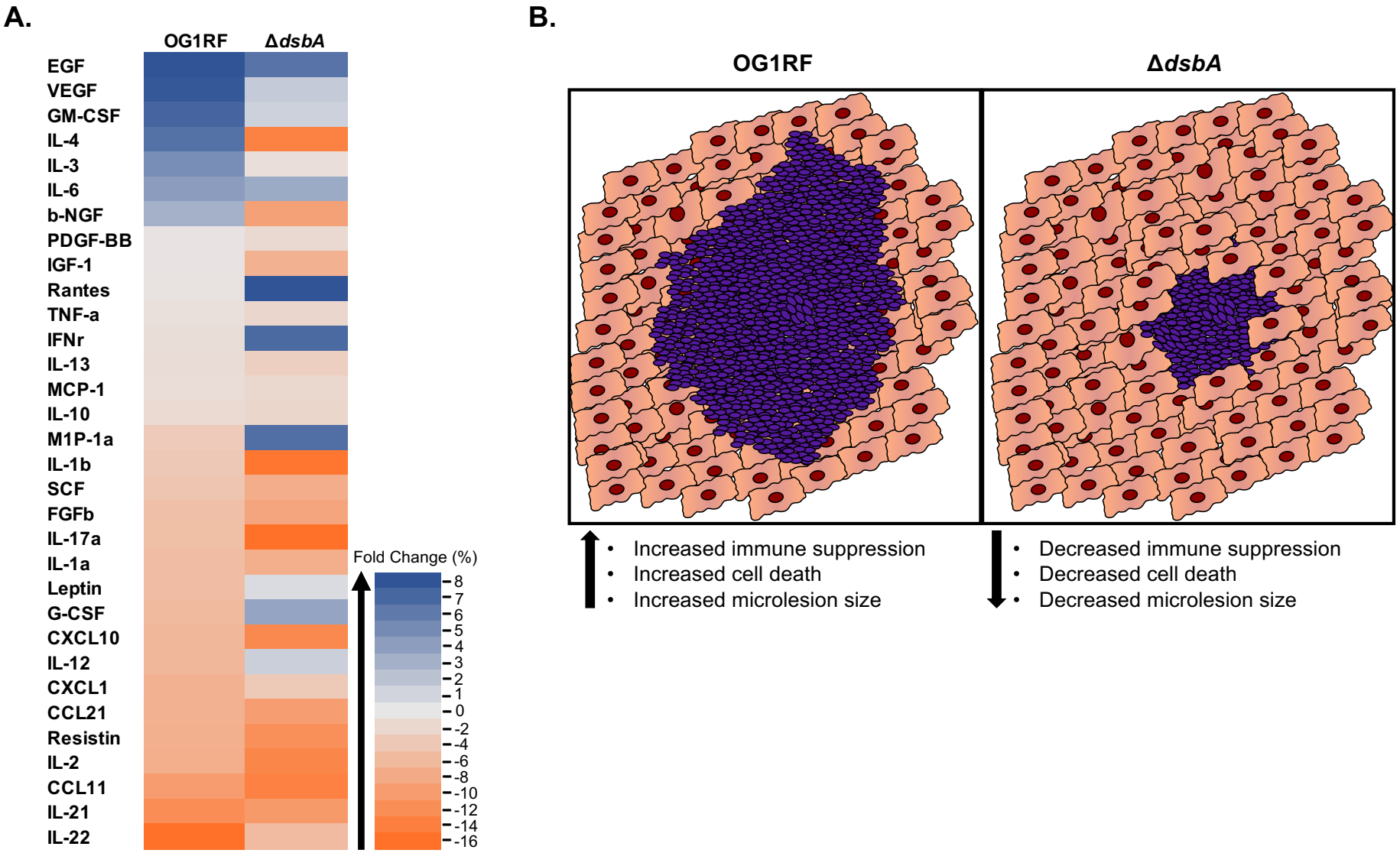
A.
OG1RF
ΔdsbA
EGF
VEGF
GM-CSF
IL-4
IL-3
IL-6
b-NGF
PDGF-BB
IGF-1
Rantes
TNF-a
IFNr
IL-13
MCP-1
IL-10
M1P-1a
IL-1b
SCF
FGFb
IL-17a
IL-1a
Leptin
G-CSF
CXCL10
IL-12
CXCL1
CCL21
Resistin
IL-2
CCL11
IL-21
IL-22
Fold Change (%)
8
7
6
5
4
3
2
1
0
-2
-4
-6
-8
-10
-12
-14
-16
B.
OG1RF
ΔdsbA
• Increased immune suppression
• Increased cell death
• Increased microlesion size
• Decreased immune suppression
• Decreased cell death
• Decreased microlesion size